

# Light-controlled topological charge in a nematic liquid crystal

Maryam Nikkhou<sup>1</sup>, Miha Škarabot<sup>1</sup>, Simon Čopar<sup>1,2</sup>, Miha Ravnik<sup>2</sup>, Slobodan Žumer<sup>1,2</sup>  
and Igor Muševič<sup>1,2\*</sup>

**Creating, imaging, and transforming the topological charge<sup>1,2</sup> in a superconductor<sup>3</sup>, a superfluid<sup>4,5</sup>, a system of cold atoms<sup>6</sup>, or a soft ferromagnet<sup>7-9</sup> is a difficult—if not impossible—task because of the shortness of the length scales and lack of control. The length scale and softness of defects in liquid crystals allow the easy observation of charges, but it is difficult to control charge creation. Here we demonstrate full control over the creation, manipulation and analysis of topological charges that are pinned to a microfibre in a nematic liquid crystal. Oppositely charged pairs are created through the Kibble–Zurek mechanism<sup>10,11</sup> by applying a laser-induced local temperature quench in the presence of symmetry-breaking boundaries. The pairs are long-lived, oppositely charged rings or points that either attract and annihilate, or form a long-lived, charge-neutral loop made of two segments with a fractional topological charge.**

Topological charge<sup>1,2</sup> is a conserved quantity that is associated with point, string or loop-like topological singularities of physical fields. It is assigned to topological defects in systems of various natures and length scales, such as Abrikosov vortices in type-II superconductors<sup>3</sup>, superfluid vortices<sup>4,5</sup> in <sup>3</sup>He and Bose–Einstein condensates<sup>6</sup>, quasiparticles in the fractional quantum Hall effect<sup>12</sup>, cold fermionic atoms in optical lattices<sup>13</sup>, and in field theories<sup>14</sup>. Integer or fractional topological charge is important for magnetization switching in soft ferromagnets<sup>7-9</sup>. In optical vortex beams the topological charge is a measure of the phase singularities of the optical field, and describes the orbital angular momentum of light<sup>15</sup>. Topological defects in liquid crystals<sup>16,17</sup> are the carriers of topological charge, which are produced as transients by a rapid pressure or temperature quench<sup>18,19</sup> and made stable either by colloidal inclusions<sup>20,21</sup>, or by confining the liquid crystal to cavities of various geometries and surface properties. One such example is liquid-crystalline droplets<sup>22,23</sup>.

Full control over the topological charge creation and manipulation in a nematic liquid crystal (NLC) is achieved by using laser tweezers to induce a thermal microquench of the NLC around an inserted thin fibre (a few  $\mu\text{m}$  in diameter). We use a focused laser beam to locally ‘melt’ and quench the NLC, which leaves behind isolated topological defects that are stabilized by the fibre. The defects appear in the form of singular points or closed loops, which can be drawn, manipulated, cut and fused together with a laser under an optical microscope. We demonstrate a direct measurement of the topological charge using the charge-induced colloidal forces. This makes inclusions in nematic liquid crystals an ideal system for studying topological charge in soft matter.

The experiments were performed on a glass fibre, a few  $\mu\text{m}$  in diameter, that was immersed in a thin layer of pentylcyanobiphenyl

(5CB) NLC, sandwiched between two glass plates. The NLC molecules were aligned uniformly parallel to the rubbing direction on the cell’s surfaces, whereas on the glass fibre they were perpendicularly aligned. We use the absorption of the focused beam of the laser tweezers to locally heat the NLC into the isotropic phase (Fig. 1a). This creates a 100  $\mu\text{m}$  diameter island of a molten (isotropic) NLC, which is rapidly quenched by shutting off the light. With no fibre inserted (Fig. 1a and Supplementary Movie 1), the island undergoes a rapid phase transition that leaves behind the phase interfaces a dense tangle of defects through a process similar to the Kibble–Zurek mechanism of defect production in the early Universe<sup>10,11,18</sup>. In less than a second, this tangle annihilates back into the uniformly ordered ground state (vacuum state).

However, there is a marked change in the outcome of the coarsening process when we perform the local melting experiment with the fibre inserted, because the connectedness of the quenching domain is changed (Fig. 1b and Supplementary Movie 2). After long times we observe two remnant topological defects, which are stabilized by the perpendicular alignment of molecules on the fibre, namely the Saturn ring<sup>24</sup> and the Saturn anti-ring, each having an opposite winding number and topological charge<sup>1,2,17</sup>, thereby preserving the charge neutrality. These rings are individually inherently stable, cannot be annihilated separately and can be arbitrarily moved with the tweezers. It should be noted that, in the absence of surface anchoring at the fibre walls, each defect would simply be allowed to pass through the NLC–fibre interface and annihilate. If left free, they slowly attract through elastic deformation of the NLC (Fig. 1c), slide towards each other along the fibre and annihilate into a non-uniform, defect-free vacuum state. By repeating the quench at different positions along the fibre, an arbitrary number of ring–anti-ring pairs can be created (Fig. 1f).

The structures of the Saturn ring and anti-ring on a fibre are modelled using the Landau–de Gennes (LdG) theory<sup>25</sup> and shown in Fig. 1d. Whereas the structure of the Saturn ring (with winding number  $-1/2$  and topological charge  $-1$  is well known<sup>17,24</sup>, the Saturn anti-ring with the opposite winding and topological charge is not stable around a sphere. A single Saturn anti-ring is stable inside a nematic droplet<sup>22,23</sup>, or in a carefully designed confinement geometry<sup>26</sup>. The sign of the topological charge of the two rings can be determined by probing the elastic deformation field around the fibre, as opposite topological charges generally attract. As a reference charge, we use a small test particle (Fig. 1e), treated for perpendicular anchoring, which is by convention assigned a  $+1$  charge for the particle and  $-1$  charge for the accompanying Saturn ring. Such a particle induces an elastic distortion that repels the equally charged part of an elastic dipole and attracts the oppositely charged part (Supplementary Movie 3).

<sup>1</sup>Condensed Matter Physics Department, Jožef Stefan Institute, Jamova 39, 1000 Ljubljana, Slovenia. <sup>2</sup>Faculty of Mathematics and Physics, University of Ljubljana, Jadranska 19, 1000 Ljubljana, Slovenia. \*e-mail: igor.musevic@ijs.si

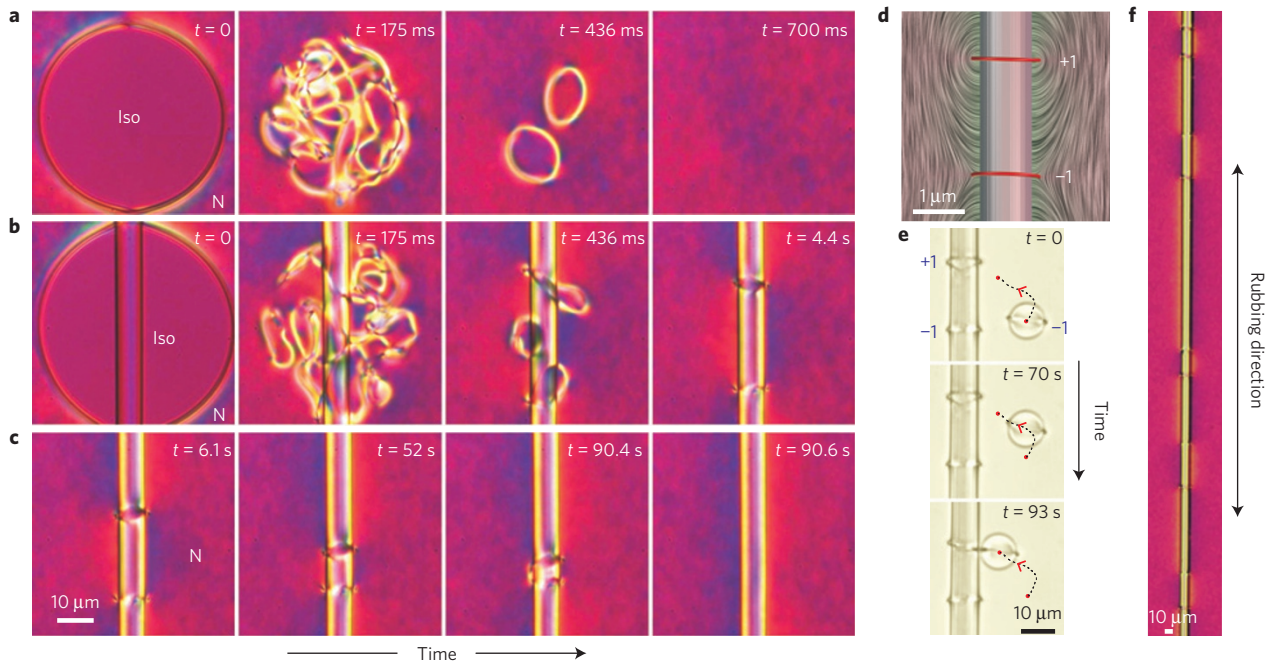


**Figure 1 | Creation and annihilation of topological charges on a fibre.** **a**, The NLC is heated into the isotropic phase by the strong light of the laser tweezers, thus creating an isotropic island (Iso). At  $t=0$  the light is switched off and the NLC is quenched into the nematic phase (N). The dense tangle of defects annihilates in less than a second. **b**, The NLC is quenched from the isotropic island surrounding a fibre. A pair of defects is created, each carrying an opposite topological charge. **c**, If let free, the pair annihilates into the vacuum. **d**, LdG simulation of the Saturn ring and the Saturn anti-ring with opposite charges and windings. **e**, The sign of the charge is tested using the repulsive force between like topological charges. **f**, An arbitrary number of ring-anti-ring pairs can be created on a fibre. Images **a-c-f** were taken between crossed polarizers and the red plate, which shows the average molecular orientation in different colours.

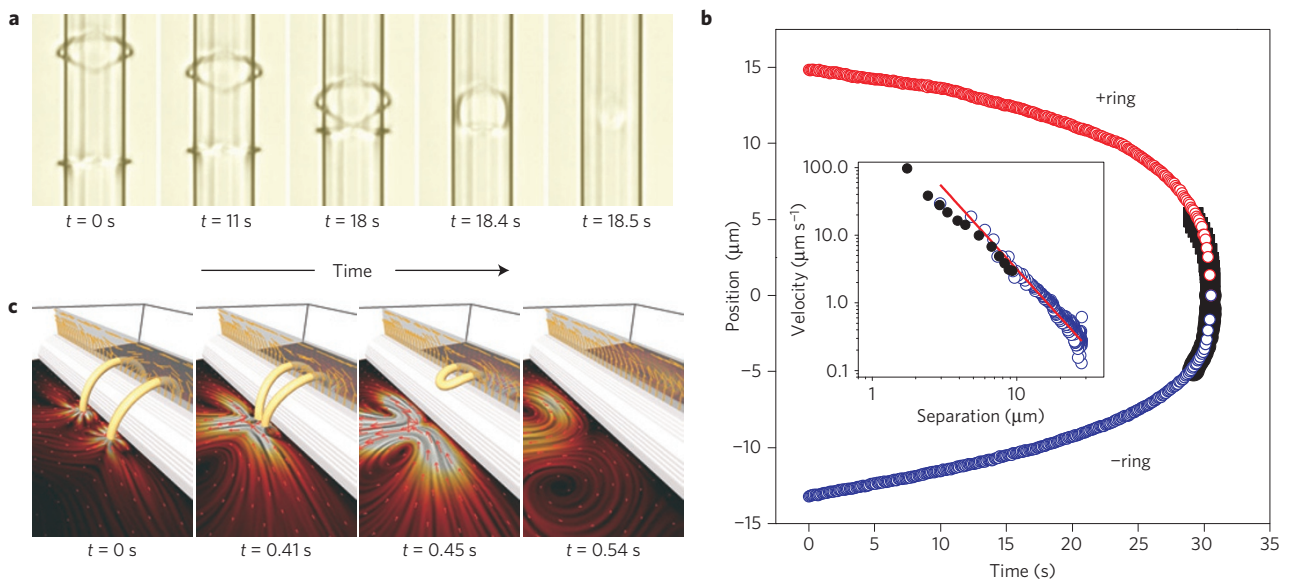


**Figure 2 | Dynamics of charge annihilation on a fibre.** **a**, A pair consisting of a Saturn ring and an anti-ring is annihilated on a fibre. The length of the fibre is  $\sim 400 \mu\text{m}$ , the diameter is  $8 \mu\text{m}$  and the cell thickness is  $65 \mu\text{m}$ . **b**, The positions of the + (red) and - (blue) Saturn rings as a function of time during pair annihilation. The inset shows the relative velocity of the two rings. The open symbols are data from the experiment; the closed symbols (black) are data from the numerical simulation. The red line is a linear fit to the blue data points. **c**, Numerical simulation of the ring and anti-ring attraction, showing the director (yellow, vertical plane) and velocity fields (red, horizontal plane).

The annihilation of rings on a fibre was analysed in thick cells (Fig. 2a and Supplementary Movie 4) by tracking their positions (Fig. 2b). The relative velocity of the rings as a function of their separation,  $d$ , shows a power-law dependence,  $v \approx 1/d^\alpha$ , with  $\alpha \approx 2.2 \pm 0.2$ , whereas the  $+1/2$  ring is faster than the  $-1/2$  ring,

$v_+/v_- \approx 1.5$ . This is similar to previous experiments on topological string attraction in nematic cells<sup>27,28</sup>, which also reported faster dynamics of defects with positive winding number. The experiments in thick cells are compared against the ring dynamics, calculated within the Beris-Edwards model of nematodynamics using the

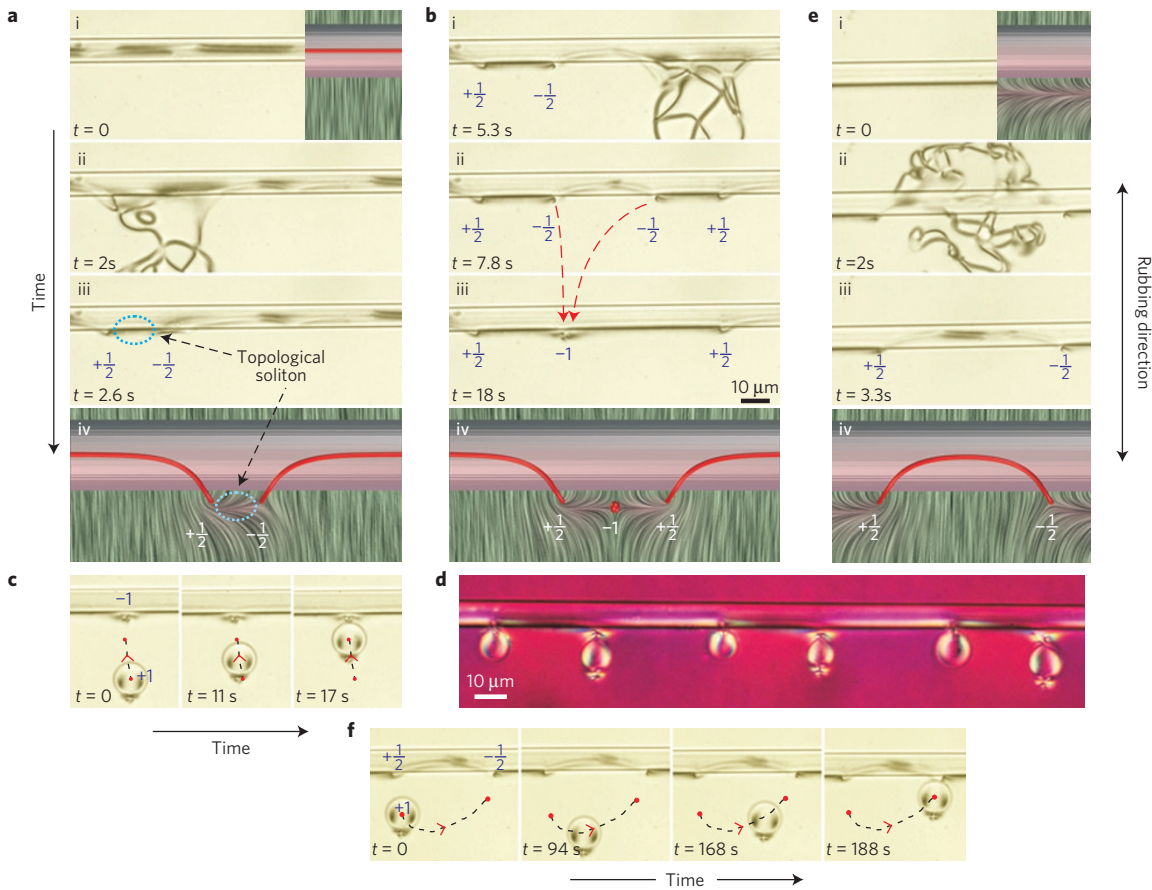


**Figure 3 | Point charges and charge-neutral loops on a fibre.** **a**, After inserting a glass fibre into a thick layer of the NLC, a gigantic Saturn ring with a  $-1$  charge is created (i). The true image is on the left; the LdG simulation is on the right. This ring is cut by the tweezers (ii), creating a narrow region of a topological soliton in between the two loops with opposite winding numbers (iii). The LdG simulation is shown in (iv). **b**, The second cut with the laser tweezers creates a second soliton on the right, isolating a closed loop in between. This loop shrinks into the  $-1$  monopole (iii). The LdG analysis demonstrates the  $-1$  monopole (hyperbolic hedgehog), with two closed loops on each side, with the winding numbers  $+1/2$  (iv). **c**, The topological charge of the  $-1$  point defect is tested with an elastic dipole. The  $+1$  part of the dipole is attracted towards the monopole on the fibre, identifying it as the  $-1$  charge. **d**, A sequence of alternating charges is created on a fibre, attracting a series of dipolar colloidal particles. **e**, A topological soliton is seen as a dark-shaded region below the fibre, and the LdG simulation is shown on the right (i). A microquench produces a long-lived charge-neutral loop, surrounded by two solitons (iii). The LdG numerical simulation of a charge-neutral loop on a fibre is shown in (iv). **f**, The charge of the charge-neutral loop is tested by the  $+1$  end of the dipolar particle. This  $+1$  end is repelled from the left section of the loop towards the right section, demonstrating oppositely charged sections.

hybrid lattice Boltzmann method<sup>29</sup> in the one-elastic-constant approximation and the material parameters of 5CB. The rings are initialized at some distance, and left to annihilate. Figure 2c shows snapshots from the simulation of the attraction and annihilation of the Saturn ring and anti-ring pair. The calculated time dependence of the  $+/-$  ring positions is shown in Fig. 2b, and is in good agreement with the experiments.

The topology of the monopoles on a fibre becomes even richer when the fibre is rotated by  $90^\circ$  and set perpendicular to the bulk orientation of the NLC. Because a fibre in the NLC is topologically equivalent to a sphere, characterized by the genus<sup>30</sup>  $g = 0$ , a single and gigantic  $-1/2$  Saturn ring is observed, which encircles the fibre all along its length (Fig. 3a and Supplementary Movie 5). This ring can be cut and reshaped, using the light of the laser tweezers, into an arbitrary number of isolated sections with different topologies and charges. As an example, Fig. 3a shows how the gigantic Saturn ring with winding number  $-1/2$  is first cut into two loops by laser tweezers. This cut locally modifies the winding number of one of the forming loops (from  $-1/2$  to  $+1/2$ ) and creates a local non-singular structure between the two loops—a distinctive topological soliton<sup>31</sup> (see also Supplementary Movie 5). After the loop on the

right is further cut into two separate loops (Fig. 3b), an isolated  $-1/2$  loop is formed that rapidly shrinks into a hedgehog with a  $-1$  charge<sup>12</sup>. This charge attracts a colloidal particle in an elastic dipolar state, where the particle carries a  $+1$  charge and the hyperbolic hedgehog a  $-1$  charge (Fig. 3c and Supplementary Movie 6). By further cutting either one of the loops, an alternating series of positive and negative point charges is created, which attract and bind dipolar colloids (Fig. 3d).

Whereas cutting the loops generates charged monopoles, an unusual topological entity is obtained by quenching the topological soliton (Fig. 3e): a closed and long-lived loop forms, which is charge neutral (Supplementary Movie 7). The far segments of this loop are similar to halves of the oppositely charged loops, which is confirmed using a test dipolar particle (Fig. 3f and Supplementary Movie 8). When the positive part of the dipole is exposed to the loop, it is repelled from the positive (left) and attracted towards the negative end of the loop. This suggests the segments are topologically independent and, in the sense of elastic interactions, act as localized opposite fractional (half) charges, although only the loop as a whole can be assigned a true topological charge. The LdG simulation of a charge-neutral loop is shown in Fig. 4a.

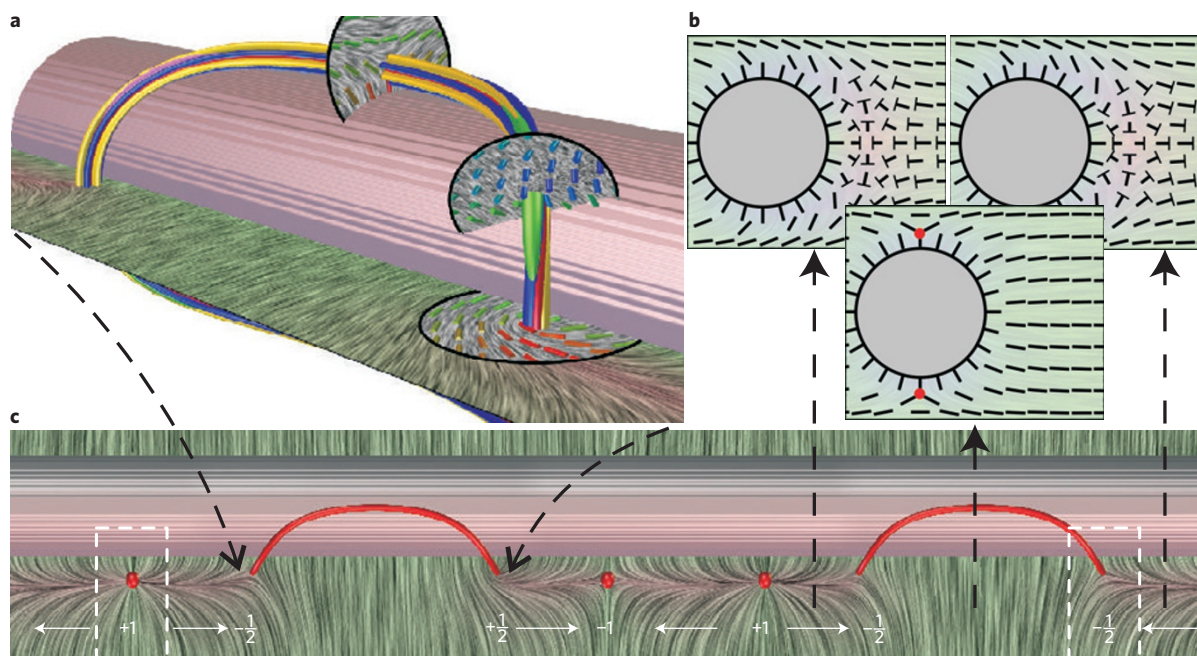


**Figure 4 | Topological rules on a fibre.** **a**, A charge-neutral loop has a  $-1/2$  winding number on one side and a  $+1/2$  on the other, with two transitions through the twist profile. The colours indicate different local structures of the loop. The yellow and blue isosurfaces indicate locations with a high bend and splay, whereas green highlights the twist deformation<sup>29</sup>. Loops of this type are freely created and annihilated, as they do not contribute to the topological charge. **b**, The fibre cross-section has three possible states: two states with an escaped disclination line of the winding number  $-1$ , with opposite escape directions, and the symmetric states with two  $-1/2$  disclinations on the top and bottom. **c**, The fibre can have any succession of the cross-sections from **b**. The transitions between cross-sections carry the topological charge, which can be assigned to entire point defects and loops, as well as to loop endings. The charge is closed in a box (two examples are shown), and the Gauss law measures the topological charge—that is, the number of escaped lines exiting the box. The direction of the topological flux depends on the direction of the escape and is shown by arrows. The topological charges are marked.

Both the creation of alternating pairs of  $+1$  and  $-1$  point charges, and the formation of charge-neutral loops are governed by a simple set of topological rules. For the sections that are translationally symmetric along the fibre, the cross-section is a two-dimensional nematic, in which the winding number is a topological invariant. Because the homeotropic fibre itself has the winding number  $+1$ , additional disclinations are required to achieve zero total winding number of the homogeneous director field far away from the fibre. This can be achieved in three different ways: with two  $-1/2$  disclination lines on the top and bottom of the fibre, or by having a soliton in the form of an escaped disclination with the winding number of  $-1$ , running on the side of the fibre, with two possible directions of escape (Fig. 4b). In the experiments we find all three configurations, interspaced by point charges and end sections of disclination loops.

In analogy with electrostatic charges, the topological charge of the loops and point defects can be determined by a Gauss law. In our system, the Gauss integral<sup>1</sup> is reduced to counting the number of topological solitons carrying the ‘topological flux’ away from or towards the defect, depending on the direction of the escape (arrows in Fig. 4c). The solitons propagate the charge and can terminate only at a topological defect. At each point, at most two of these solitons can meet, so the only possible charges are the  $+1$  and  $-1$  point defects, and the  $+1/2$  and  $-1/2$  fractional charges, assigned to the end sections of the loops (Fig. 4c). A whole loop can either have same-signed ends and be topologically equivalent to one of the point monopoles, or have opposite-signed ends, amounting to a zero total charge (Fig. 4a). Close observation of the director reveals that the loop ending with the  $+1/2$  topological charge also has a  $+1/2$  winding number, and vice versa. This is specific to the geometry of our fibre, whereas a general correspondence between the winding numbers and the topological charges requires a careful theoretical understanding<sup>32</sup>.

This work solves the long-standing problem of the controlled creation, manipulation and analysis of topological charges in liquid crystals. We have shown that any even number of topological charges could be deliberately created on topologically simple objects, which opens new routes to the design and assembly of topologically complex colloidal structures. We believe that the strategy developed here could be applied to topological charges in spin systems, magnetic materials and charge-density waves<sup>33</sup>. More broadly, this work demonstrates the sensitivity of the Kibble–Zurek mechanism and the coarsening dynamics of entangled defects at late times to the connectedness of space and symmetry-breaking boundary conditions, which might have implications also on the cosmological level. Finally, the nematic liquid crystal with inclusions is a unique platform for studying the central topological invariants of the ordering fields.

Received 9 July 2014; accepted 13 November 2014;  
published online 22 December 2014

## References

- Mermin, N. D. The topological theory of defects in ordered media. *Rev. Mod. Phys.* **51**, 591–603 (1979).
- Chaikin, P. M. & Lubensky, T. C. *Principles of Condensed Matter Physics* (Cambridge Univ. Press, 1995).
- Bishop, D. J., Gammel, P. L., Huse, D. A. & Murray, C. A. Magnetic flux line lattices and vortices in the copper oxide superconductors. *Science* **255**, 165–172 (1992).
- Mermin, N. D. & Ho, T.-L. Circulation and angular momentum in the A phase of superfluid helium-3. *Phys. Rev. Lett.* **36**, 594–597 (1976).
- Ruutu, V. M. H. *et al.* Vortex formation in neutron-irradiated superfluid  $^3\text{He}$  as an analogue of cosmological defect formation. *Nature* **382**, 334–336 (1996).
- Weiler, C. N. *et al.* Spontaneous vortices in the formation of Bose–Einstein condensates. *Nature* **455**, 948–952 (2008).

7. Wachowiak, A. *et al.* Direct observation of internal spin structure of magnetic vortex cores. *Science* **298**, 577–580 (2002).
8. Tchernyshyov, O. & Chern, G.-W. Fractional vortices and composite domain walls in flat nanomagnets. *Phys. Rev. Lett.* **95**, 197204 (2005).
9. Choe, S.-B. *et al.* Vortex core-driven magnetization dynamics. *Science* **304**, 420–422 (2004).
10. Kibble, T. W. B. Topology of cosmic domains and strings. *J. Phys. A* **9**, 1387–1398 (1976).
11. Zurek, W. H. Cosmological experiments in condensed matter physics. *Phys. Rep.* **276**, 177–221 (1996).
12. Van Heck, B., Burrello, M., Yacoby, A. & Akhmerov, A. R. Topological blockade and measurement of topological charge. *Phys. Rev. Lett.* **110**, 086803 (2013).
13. Wang, L., Troyer, M. & Dai, X. Topological charge pumping in a one-dimensional optical lattice. *Phys. Rev. Lett.* **111**, 026802 (2013).
14. Patani, A., Schindwein, M. & Shafi, Q. Topological charges in field theory. *J. Phys. A* **9**, 1513–1520 (1976).
15. Allen, L., Beijersbergen, M. W., Spreeuw, R. J. C. & Woerdman, J. P. Orbital angular momentum of light and the transformation of Laguerre-Gaussian laser modes. *Phys. Rev. A* **45**, 8185–8189 (1992).
16. Kurik, M. V. & Lavrentovich, O. D. Defects in liquid crystals: Homotopy theory and experimental studies. *Sov. Phys. Usp.* **154**, 381–431 (1988).
17. Alexander, G. P., Chen, B. G., Matsumoto, E. A. & Kamien, R. D. Disclination loops, point defects, and all that in nematic liquid crystals. *Rev. Mod. Phys.* **84**, 497–514 (2012).
18. Chuang, I., Durrer, R., Turok, N. & Yurke, B. Cosmology in the laboratory: Defect dynamics in liquid crystals. *Science* **251**, 1336–1342 (1991).
19. Bowick, M. J., Chandar, L., Schiff, E. A. & Srivasava, A. M. The cosmological Kibble mechanism in the laboratory: String formation in liquid crystals. *Science* **263**, 943–945 (1994).
20. Poulin, P., Stark, H., Lubensky, T. C. & Weitz, D. A. Novel colloidal interactions in anisotropic fluids. *Science* **275**, 1770–1773 (1997).
21. Muševič, I., Škarabot, M., Tkalec, U., Ravnik, M. & Žumer, S. Two-dimensional nematic colloidal crystals self-assembled by topological defects. *Science* **313**, 954–958 (2006).
22. Volovik, G. E. & Lavrentovich, O. D. Topological dynamics of defects: Boojums in nematic drops. *Sov. Phys. JETP* **58**, 1159–1166 (1983).
23. Lavrentovich, O. D. Topological defects in dispersed liquid crystals, or words and worlds around liquid crystal drops. *Liq. Cryst.* **24**, 117–125 (1998).
24. Terentjev, E. M. Disclination loops, standing alone and around solid particles in nematic liquid crystals. *Phys. Rev. E* **51**, 1330–1337 (1995).
25. De Gennes, P. G. & Prost, J. *The Physics of Liquid Crystals* 2nd edn (Oxford Science Publications, 1993).
26. Cavallaro, M. *et al.* Exploiting imperfections in the bulk to direct assembly of surface colloids. *Proc. Natl Acad. Sci. USA* **110**, 18804–18808 (2013).
27. Blanc, C., Svenšek, D., Žumer, S. & Nobili, M. Dynamics of nematic liquid crystal disclinations: The role of the backflow. *Phys. Rev. Lett.* **95**, 097802 (2005).
28. Dierking, I. *et al.* Anisotropy in the annihilation dynamics of umbilic defects in nematic liquid crystals. *Phys. Rev. E* **85**, 021703 (2012).
29. Beris, A. N. & Edwards, B. J. *Thermodynamics of Flowing Systems* (Oxford Univ. Press, 1994).
30. Senyuk, B. *et al.* Topological colloids. *Nature* **493**, 200–205 (2013).
31. Kleman, M. & Lavrentovich, O. D. Topological point defects in nematic liquid crystals. *Phil. Mag.* **86**, 4117–4137 (2006).
32. Čopar, S. Topology and geometry of nematic braids. *Phys. Rep.* **538**, 1–37 (2014).
33. Yusupov, P. *et al.* Coherent dynamics of macroscopic electronic order through a symmetry breaking transition. *Nature Phys.* **6**, 681–684 (2010).

### Acknowledgements

The authors acknowledge stimulating discussions with R. D. Kamien. The work was supported by the Slovenian Research Agency (ARRS) under contracts P1-0099, J1-6723, Z1-5441 and Z1-6725, and in part by the Centre of Excellence NAMASTE, EC Marie Curie project HIERARCHY (PITN-GA-2008-215851) and FP7-PEOPLE-2011-CIG grant FREEFLUID (Project No: 304040).

### Author contributions

M.N. performed the experiments, M.Š. and M.N. analysed the experiments. S.Č. performed topological analysis and numerical modelling, M.R. performed numerical simulation of annihilation dynamics, S.Ž. supervised modelling, I.M. initiated and supervised the experimental work and wrote the main manuscript. All authors contributed to the final version of the manuscript.

### Additional information

Supplementary information is available in the [online version of the paper](#). Reprints and permissions information is available online at [www.nature.com/reprints](http://www.nature.com/reprints). Correspondence and requests for materials should be addressed to I.M.

### Competing financial interests

The authors declare no competing financial interests.